Appendix S1 Phylogenetic analyses and species sampling, patterns of lineage diversification and morphological evolution through time

Our nuclear sampling consisted of 18 of 20 extant parrotbill species and different subspecies for several polytypic species, following the taxonomy of Robson (2007) with the exception of *Paradoxornis margaritae* and *P. przewalskii* (Table S1). *Panurus biarmicus* has for a long time been included in Paradoxornithidae (Robson, 2007), but has been recently shown to be only distantly related to this clade (Alström *et al.*, 2006). Hence, it was not included in our analyses.

It should be taken into account that some of the allopatric populations of different parrotbill species have recently been upgraded from subspecies to species based on morphological features (Penhallurick & Robson, 2009; Gill, 2014). This increased species number, however, would have no influence on our conclusions on diversification patterns. First, it would not alter our inferences on morphological evolution because subspecies differ mainly in plumage patterns and not in size and structure. Second, we assume no influence on our conclusions on the history of climate niche evolution, because the split of subspecies to species only concerns recent events and hence merely affects very young clades. Biogeographic inferences could be more resolved towards the present however, but it would not change the results for deeper nodes.

We used DNA sequences for the different species of the two mitochondrial genes cytochrome b (cytb, 1042 base pairs (bp)) and NADH dehydrogenase subunit 2 (ND2, 1041 bp), and two nuclear loci, the nuclear recombination activating gene 1 (RAG1, 962 bp), and the nuclear intron 2 of archain (ARCN1, 742 bp), and the Z-linked intron 5 of ADAM metal lopeptidase with thrombospondin type 1 motif, 6 variant 2 (ADAMTS6, 550 bp). These sequences were retrieved from Yeung et al. (2011). The overall dataset contained 4337 bp for each species.

Sequences of the different markers were aligned using the MAFFT algorithm (Katoh *et al.*, 2002) as implemented in GeneiousPro 7.0.6 (Drummond *et al.*, 2011). To infer a species tree from the five analyzed markers, we used the multispecies coalescent algorithm *BEAST as implemented in BEAST 1.7.5 (Drummond & Rambaut, 2007; Heled & Drummond, 2010). The different species and their subspecies were defined *a priori* as ‘species’ following the

taxonomy of Robson (2007). We used different substitution, clock and tree models for the three nuclear markers, while the two mtDNA markers were assigned the same substitution, clock and tree model. Best-fitting substitution models were evaluated with Modeltest (Posada & Crandall, 1998), as implemented in GeneiousPro. A Yule process on species trees was implemented in all analyses, and we used a relaxed uncorrelated lognormal distribution for the different partitions. To calibrate the species tree, we implemented a substitution rate for the mtDNA, using the robust overall divergence rate of 2.1 per million year (Ma) (0.0105 substitution/site/Ma)(Weir & Schluter, 2008), of 0.00135 substitution/site/Ma for the two nuclear markers (Ellegren, 2007; Smith *et al.*, 2013) and of 0.00145 substitution/site/Ma for the sex-linked marker (Ellegren, 2007). These values were used as means for a lognormal prior distribution with a wide logarithmic standard deviation of 0.2. The MCMC analysis was run five times independently for 50 million generations with sampling every 1000 generations. TRACER 1.5 (Rambaut & Drummond, 2007) was used to confirm appropriate burn-in and the adequate effective sample sizes (ESS) of the posterior distribution, and to compare likelihoods and posterior probabilities of all parameters to assess convergence among the five independent runs. The log and tree files from the different runs were combined with LogCombiner 1.7.5 with a burn-in of 15 million generations each. The resulting maximum clade credibility species tree and the 95% highest posterior density (HPD) distributions of each estimated node were calculated with Tree Annotator 1.7.5 (Drummond & Rambaut, 2007) and visualized using FIGTREE 1.2. (Rambaut, 2008).

The comparison of the five independent *BEAST runs revealed convergence of all parameters. When combined with a 15 million generations burn-in each, the resulting effective sample sizes for parameters were > 200, with the exception of five population size parameters with effective sample sizes between 117 and 174. The maximum clade credibility species tree was then computed from 175,005 trees (Fig. 2).

The R packages ‘Laser’ v. 2.4.1 (Rabosky, 2006a), ‘Geiger’ v. 2.0.1 and v. 1.99-3 (Harmon *et al.*, 2008) and ‘Phytools’ 0.9-93 (Revell, 2012) were used for all comparative data modeling.

Temporal variation in diversification rates within parrotbills was visualized with semi logarithmic lineage-through-time plots (LTT). We used the mean from the posterior

distribution of trees from the *BEAST analyses and plotted the 95% confidence interval of the lineages given at a time in the past from 1000 trees randomly chosen from the posterior distribution of the *BEAST analyses.

To test whether diversification rates have decreased over time, we calculated the gamma (γ) statistic of Pybus & Harvey (2000). The sensitivity of the inferred gamma value was assessed with the Monte Carlo Constant rate test (MCCR), based on 10, 000 simulated phylogenies, taking into account incomplete taxon sampling.

Different likelihood models for diversification rates were moreover fitted on the maximum clade credibility species tree from the *BEAST analyses (Rabosky, 2006b; Rabosky & Lovette, 2008) (Table 1). AIC (Akaike information criterion) scores were compared among the following models: 1) a pure birth (Yule); 2) birth-death (bd); 3) bd rate-variable model with the speciation rate λ_1 shifting to λ_2 at a time t (yule2rate); 4) yule3rate; 5) a yule4rate; 6) exponential diversity-dependent (DDX) and 7) logistic diversity-dependent (DDL) speciation rate model; 8) model with exponentially declining speciation rate through time (constant extinction, SPVAR); 9) exponentially increasing extinction rate through time (constant speciation, EXVAR); 10) varying speciation and extinction rates through time (BOTHVAR). An increase in model fit was overall considered as significant when the reduction in AIC score in a more complex model was ≥ 2 (Burnham & Anderson, 2002).

The gamma (γ) statistic was -1.458 with a P-value of 0.095, as assessed with the Monte Carlo Constant Rate test (MCCR). Hence, we detected no evidence for a significant slowdown of diversification rate over time.

A yule2rate model was found to be the best-fitting model of lineage diversification, with a slight increase in speciation rate shortly before the present when considering ΔAIC, and was significantly different against an overall constant diversification rate over time (Table S3). When considering ΔAICc instead, a DDX model was found to be best fitting, although it was not significantly different from a pure birth model.

We additionally fitted six likelihood models of continuous morphological evolution to our data and compared their AIC scores, based on the maximum clade credibility species tree. The models were: 1) Brownian motion (BM); 2) Ornstein-Uhlenbeck (OU) (Butler & King, 2004); 3)

a time-dependent linear model (TDL), with linear rate change through time; 4) time-dependent early-burst (EB) model, with exponential rate change through time (Harmon *et al.*, 2010); 5) a diversity-dependent linear model (DDL), with its rate changing linearly with changing species diversity in a clade (Weir & Mursleen, 2012); 6) a diversity-dependent linear model (DDX), with its rate changing exponentially with changing species diversity in a clade (Weir & Mursleen, 2012).

Appendix S2 Ecological niche modeling and niche overlaps and equivalency

Occurrence records of each parrotbill species were obtained from two sources: 1) field observation records from the online database "China Bird Report" (http://www.birdreport.cn/) and Li et al. (2013); 2) occurrences from the Global Biodiversity Information Facility database (GBIF; http://www.gbif.org/). All records were mapped using ArcGIS 9.2 (ESRI, Redland, CA) for visual inspection. We detected duplicates and possible errors in georeferencing by double-checking in spreadsheets and geographic information systems (GIS). Because models using only presence data can be affected by sample selection bias (Phillips *et al.*, 2009) and spatial autocorrelation, we created a 0.1°-resolution grid in which we included only a single randomly selected occurrence per grid-cell. This spatial filtering yielded 1, 260 unique georeferenced records from throughout the entire distribution ranges of all species. This stratification enhanced our ability to model the unbiased potential distribution of species and avoided a prediction biased by sampling effort (Soberon & Nakamura, 2009). Consequently, the number of occurrences per species ranged from 1 (*P. przewalskii*) to 715 (*P. webbianus*). *P. przewalskii* and *P. flavirostris* (N = 3) were excluded when ecological niche models (ENMs) were constructed, due to the small sample size of occurrences.

We obtained 19 bioclimatic variables, representing climatic conditions (the period 1950-2000) within the study area with a resolution of 0.1 arc-degrees from the WorldClim database v.1.4 (Hijmans *et al.*, 2005). Including all bioclimatic variables in ENMs might cause 'over-fitting' problems and uncertainties due to high degrees of co-linearity among variables, especially for small sample sizes of occurrences (Heikkinen *et al.*, 2006; Hu & Jiang, 2010). Therefore, we

first carried out Pearson's correlation tests and jackknife analyses in ENM, and retained the variables that gave a higher value in the percent contribution to the Maxent model (Phillips *et al.*, 2006; Hu & Liu, 2014) for highly correlated variable pairs ($|r| \geq 0.8$). Consequently, seven variables were retained as predictors for further analyses: annual mean temperature (T_{anu}), mean monthly temperature range (T_{ran}), temperature seasonality (T_{sea}), annual precipitation ($Prec_{anu}$), precipitation in the driest month ($Prec_{dry}$), precipitation seasonality ($Prec_{sea}$), precipitation in the coldest quarter ($Prec_{col}$).

We used the maximum entropy algorithm employed in Maxent 3.3.3k (Phillips *et al.*, 2006) to construct ENMs for each species. Discrimination abilities of the ENMs were assessed by computing the area under the receiver operating characteristic curve (AUC) (Swets, 1988). We mainly employed default settings and ran models with 10 bootstrap replicates, using 70% of the occurrences for model training and 30% for testing the resulting models. To provide robust projections in climatic suitability, the replicates from Maxent were used as proxy-models to constitute the consensus-based ensemble-forecasting (Araujo & New, 2007). The averages across all replicates were obtained for further processing by calculating within each grid-cell in ArcGIS 9.2 (ESRI, Redland, CA). An easily interpretable logistic output format was selected with suitability values ranging from 0 (lowest) to 1 (highest) (Phillips & Dudik, 2008).

To evaluate the niche overlap between species, we calculated two indices, i.e. Schoener's *D* and *I* (Warren et al. 2008). These values measured the similarity of projected suitability for each grid cell of the study area and ranged from 0 (no niche overlap) to 1 (complete overlap). The estimates of *D* and *I* were obtained by comparing projected suitability from Maxent for each grid cell of the study area, after normalizing each ENM (Warren *et al.*, 2008). We used a niche identity test to test if ENMs of species are distributed in identical environmental space (Warren *et al.*, 2008). We pooled occurrences and randomized their identities by 100 replicates to produce two new samples with the same number of observations as the empirical data. This helped to generate a pseudo-replicated null distribution. The observed similarity values were compared with this null distribution of values of random replicates to determine whether species are more different than would be expected by chance. The null hypothesis of niche identity is rejected when the empirically observed value for *D* or *I* is

significantly different from the pseudo-replicated data sets. We calculated the values of *D* and *I* in ENMTools 1.3 (Warren *et al.*, 2008, 2010).

References

Alström, P., Ericson, P.G.P., Olsson, U. & Sundberg, P. (2006) Phylogeny and classification of the avian superfamily Sylvioidea. *Molecular Phylogenetics and Evolution*, **38**, 381-397.

Araujo, M.B. & New, M. (2007) Ensemble forecasting of species distributions. *Trends in Ecology and Evolution*, **22**, 42-47.

Baur, H. & Leuenberger, C. (2011) Analysis of ratios in multivariate morphometry. *Systematic Biology*, **60**, 813-825.

Burnham, K.P. & Anderson, D.R. (2002) *Model selection and mulitimodel inference (2nd edition)*.. Springer-Verlag, New York.

Drummond, A.J. & Rambaut, A. (2007) BEAST: Bayesian evolutionary analysis by sampling trees. *BMC Evolutionary Biology*, **7,** 214.

Drummond, A.J., Ashton, B., Buxton, S., Cheung, M., Cooper, A., Duran, C., Field, M., Heled, J., Kearse, M., Markowitz, S., Moir, R., Stones-Havas, S., Sturrock, S., Thierer, T. & Wilson, A. (2011) *Geneious v5.4*. Available from: http://www.geneious.com/.

Ellegren, H. (2007) Molecular evolutionary genomics of birds. *Cytogenetic and Genome Research*, **117**, 120-130.

Harmon, L.J., Weir, J.T., Brock, C.D., Glor, R.E. & Challenger, W. (2008) GEIGER: investigating evolutionary radiations. *Bioinformatics*, **24**, 129-131.

Heikkinen, R.K., Luoto, M., Araujo, M.B., Virkkala, R., Thuiller, W. & Sykes, M.T. (2006) Methods and uncertainties in bioclimatic envelope modelling under climate change. *Progress in Physical Geography*, **30**, 751-777.

Heled, J. & Drummond, A.J. (2010) Bayesian inference of species trees from multilocus data. *Molecular Biology and Evolution*, **27**, 570-580.

Hijmans, R.J., Cameron, S.E., Parra, J.L., Jones, P.G. & Jarvis, A. (2005) Very high resolution interpolated climate surfaces for global land areas. *International Journal of Climatology*, **25**, 1965-1978.

Hu, J. & Jiang, Z. (2010) Predicting the potential distribution of the endangered Przewalski's gazelle. *Journal of Zoology*, **282**, 54-63.

Hu, J.H. & Liu, Y. (2014) Unveiling the conservation biogeography of a data-deficient endangered bird species under climate change. *PLoS ONE*, **9**, e84529

Katoh, K., Misawa, K., Kuma, K. & Miyata, T. (2002) MAFFT: a novel method for rapid multiple sequence alignment based on fast Fourier transform. *Nucleic Acids Research*, **30**, 3059-3066.

Li, X. Y., Liang, L., Gong, P., Liu, Y., Yang, F.F. (2013) Bird watching in China reveals bird distribution changes. C*hinese Science Bulletin*, **58**, 649-656.

Phillips, S.J. & Dudik, M. (2008) Modeling of species distributions with Maxent: new extensions and a comprehensive evaluation. *Ecography*, **31**, 161-175.

Phillips, S.J., Anderson, R.P. & Schapire, R.E. (2006) Maximum entropy modeling of species geographic distributions. *Ecological Modelling*, **190**, 231-259.

Phillips, S.J., Dudik, M., Elith, J., Graham, C.H., Lehmann, A., Leathwick, J. & Ferrier, S. (2009) Sample selection bias and presence-only distribution models: implications for background and pseudo-absence data. *Ecological Applications*, **19**, 181-197.

Posada, D. & Crandall, K.A. (1998) MODELTEST: testing the model of DNA substitution. *Bioinformatics*, **14**, 817-818.

Pybus, O.G. & Harvey, P.H. (2000) Testing macro-evolutionary models using incomplete molecular phylogenies. *Proceedings of the Royal Society B-Biological Sciences*, **267**, 2267-2272.

Rabosky, D.L. (2006a) LASER: a maximum likelihood toolkit for detecting temporal shifts in diversification rates from molecular phylogenies. *Evolutionary Bioinformatics Online*, **2**, 257-260.

Rabosky, D.L. (2006b) Likelihood methods for detecting temporal shifts in diversification rates. *Evolution*, **60**, 1152-1164.

Rabosky, D.L. & Lovette, I.J. (2008) Explosive evolutionary radiations: decreasing speciation or increasing extinction through time? *Evolution*, **62**, 1866-1875.
Rambaut, A. (2008) *FigTree 1.2., published by the author.*
Rambaut, A. & Drummond, A.J. (2007) Tracer v1.5, available from http://beast.bio.ed.ac.uk/Tracer.
Revell, L.J. (2012) phytools: an R package for phylogenetic comparative biology (and other things). *Methods in Ecology and Evolution*, **3**, 217-223.
Robson, C. (2007) Familiy Paradoxornithidae (Parrotbills). *Handbook of the birds of the world* (ed. by J. Del Hoyo, A. Elliott, J. Sargatal and D.A. Christie), pp. 292-321. Lynx Edicions, Barcelona.
Smith, B.T., Ribas, C.C., Whitney, B.M., Hernnndez-Banos, B.E. & Klicka, J. (2013) Identifying biases at different spatial and temporal scales of diversification: a case study in the Neotropical parrotlet genus *Forpus*. *Molecular Ecology*, **22**, 483-494.
Soberon, J. & Nakamura, M. (2009) Niches and distributional areas: Concepts, methods, and assumptions. *Proceedings of the National Academy of Sciences of the United States of America*, **106**, 19644-19650.
Swets, J.A. (1988) Measuring the accuracy of diagnostic systems. *Science*, **240**, 1285-1293.
Warren, D.L., Glor, R.E. & Turelli, M. (2008) Environmental niche equivalency versus conservatism: quantitative approaches to niche evolution. *Evolution*, **62**, 2868-2883.
Warren, D.L., Glor, R.E. & Turelli, M. (2010) ENMTools: a toolbox for comparative studies of environmental niche models. *Ecography*, **33**, 607-611.
Weir, J.T. & Schluter, D. (2008) Calibrating the avian molecular clock. *Molecular Ecology*, **17**, 2321-2328.
Yeung, C.K.L., Lin, R.C., Lei, F.M., Robson, C., Hung, L.M., Liang, W., Zhou, F.S., Han, L.X., Li, S.H. & Yang, X.J. (2011) Beyond a morphological paradox: Complicated phylogenetic relationships of the parrotbills (Paradoxornithidae, Aves). *Molecular Phylogenetics and Evolution*, **61**, 192-202.

Appendix S3 Tables S1-S3, Figures S1-S5

Table S1 Parrotbill species sampled and associated GenBank accession numbers for the five genes analyzed in this study.

Taxon	Range	Voucher	Cytb	ND2	RAG-1	ARCN1	ADAMTS6
Paradoxornis webbianus bulomachus	Hwalian, Taiwan, China	NTNU T0666	JF756694	JF756768	JF756876	JF756917	JF756958
Paradoxornis webbianus bulomachus	Hwalian, Taiwan, China	NTNU T2225	JF756695	JF756769	JF756853	JF756894	JF756935
Paradoxornis webbianus suffusus	Foping, Shaanxi, China	NMNS T5537/NTNU T0834	JF756698	JF756772	JF756878	JF756919	JF756960
Paradoxornis webbianus suffusus	Foping, Shaanxi, China	NMNS T5539/NTNU T0836	JF756699	JF756773	JF756879	JF756920	JF756961
Paradoxornis webbianus suffusus	Foping, Shaanxi, China	NMNS T137/NTNU T3158	JF756700	JF756774	JF756862	JF756903	JF756944
Paradoxornis webbianus suffusus	Foping, Shaanxi, China	NMNS T155/NTNU T3159	JF756701	JF756775	JF756863	JF756904	JF756945
Paradoxornis alphonsianus alphonsianus	Kaili, Guizhou, China	NTNU T4285	JF756708	JF756782	JF756865	JF756906	JF756947
Paradoxornis alphonsianus alphonsianus	Kaili, Guizhou, China	NTNU T4290	JF756709	JF756783	JF756866	JF756907	JF756948
Paradoxornis alphonsianus yunnanensis	Kunming, Yunnan, China	NTNU T1634	JF756710	JF756784	JF756847	JF756888	JF756929
Paradoxornis brunneus ricketti	W Yunnan, China	NTNU 3091	JF756714	JF756788	JF756859	JF756900	JF756941
Paradoxornis brunneus ricketti	Lijian, Yunnan, China	NTNU T5450	JF756717	JF756791	JF756871	JF756912	JF756953
Paradoxornis brunneus ricketti	Lijian, Yunnan, China	NTNU T5451	JF756718	JF756792	JF756872	JF756913	JF756954
Paradoxornis conspicillatus	Foping, Shaanxi, China	NMNS T5581/NTNU T0878	JF756720	JF756794	JF756881	JF756922	JF756963
Paradoxornis nipalensis nipalensis	Gonga, Nepal	AMNS JGG1062/NTNU T2901	JF756726	JF756800	JF756858	JF756899	JF756940
Paradoxornis nipalensis poliotis	Gaoligongshan, Yunnan, China	KIZ GLGS1422/NTNU T2668	JF756727	JF756801	JF756856	JF756897	JF756938
Paradoxornis verreauxi craddocki	Vietnam	NTNU T1781	JF756729	JF756803	JF756849	JF756890	JF756931
Paradoxornis verreauxi craddocki	Vietnam	NTNU T1783	JF756730	JF756804	JF756850	JF756891	JF756932
Paradoxornis verreauxi morrisonianus	Mt. Ho-Huan, Taiwan, China	NTNU T0073	JF756731	JF756805	JF756877	JF756918	JF756959
Paradoxornis fulvifroms albifacies	Gaoligongshan, Yunnan, China	KIZ GLGS426/NTNU T0968	JF756733	JF756807	JF756882	JF756923	JF756964
Paradoxornis fulvifroms albifacies	Gaoligongshan, Yunnan, China	KIZ GLGS2258/NTNU T2666	JF756734	JF756808	JF756855	JF756896	JF756937

Paradoxornis fulvifroms cyanophrys	Foping, Shaanxi, China	NMNS T164/NTNU T3151	JF756735	JF756809	JF756860	JF756901	JF756942
Paradoxornis fulvifroms cyanophrys	Foping, Shaanxi, China	NMNS T166/NTNU T3152	JF756736	JF756810	JF756861	JF756902	JF756943
Paradoxornis guttaticollis	Vietnam	NTNU T1797	JF756738	JF756812	JF756851	JF756892	JF756933
Paradoxornis gularis fokiensis	Jinxiu, Guanxi, China	KIZ DYS081/NTNU T5452	JF756744	JF756818	JF756873	JF756914	JF756955
Paradoxornis gularis fokiensis	Jinxiu, Guanxi, China	KIZ DYS082/NTNU T5453	JF756745	JF756819	JF756874	JF756915	JF756956
Paradoxornis gularis transfluvialis	Vietnam	NTNU T1816	JF756746	JF756820	JF756852	JF756893	JF756934
Paradoxornis gularis transfluvialis	Quan Nam, Vietnam	AMNH PRS2212/NTNU T2899	JF756747	JF756821	JF756857	JF756898	JF756939
Paradoxornis paradoxus	Foping, shanxi, China	NMNS T5452/NTNU T1255	JF756751	JF756825	JF756843	JF756884	JF756925
Paradoxornis paradoxus	Foping, shanxi, China	NMNS T5451/NTNU T1256	JF756752	JF756826	JF756844	JF756885	JF756926
Paradoxornis unicolor	Yunnan, China	NTNU T1683	JF756753	JF756827	JF756845	JF756889	JF756930
Paradoxornis unicolor	Gaoligongshan, Yunnan, China	KIZ GLGS5058/NTNU T5108	JF756756	JF756830	JF756868	JF756909	JF756950
Paradoxornis unicolor	Lushui, Yunnan, China	KIZ GLGS5057/NTNU T5252	JF756757	JF756831	JF756870	JF756911	JF756952
Conostoma aemodium	Foping, Shaanxi, China	NMNS T38/NTNU T4512	JF756760	JF756834	JF756867	JF756908	JF756949
Conostoma aemodium	Foping, Shaanxi, China	NMNS T10108/NTNU T5219	JF756761	JF756835	JF756869	JF756910	JF756951

Table S2 Individuals and measurements used for morphological analyses.

Species	Subspecies	Voucher	Length of bill (BSk)	Width of bill (BWF)	Depth of bill (Bmax)	Tail length (TL)	Tarsus length (TaL)
Conostoma aemodium	monotypic	IOZ45095	22.25	11.20	13.20	125	38.01
		IOZ17081	22.52	10.85	13.60	135	37.12
		IOZ35566	23.76	10.22	14.60	129	39.03
		IOZ49704	22.27	10.85	13.56	118	36.84
Paradoxornis paradoxus	*paradoxus*	IOZ49711	15.71	7.35	11.57	104	28.25
		IOZ35562	15.65	7.47	11.36	103	29.60
		IOZ35561	15.34	7.22	11.17	91	26.61
		IOZ17708	15.82	7.54	11.31	111	28.52
Paradoxornis unicolor	monotypic	IOZ35558	13.73	7.02	10.57	100	29.56
		IOZ35559	14.33	7.03	10.67	106	/
		IOZ46494	14.39	7.00	10.81	119	29.96
		IOZ46495	14.17	7.09	10.56	116	30.24
Paradoxornis guttaticollis	monotypic	IOZ57250	17.09	8.39	16.03	100	26.23
		IOZ57251	16.24	8.32	15.57	101	25.74
		IOZ57252	16.46	8.30	15.26	95	25.87
		IOZ57255	17.61	8.37	16.11	106	26.00
		IOZ57257	17.63	8.40	16.13	99	26.35
		IOZ23429	17.53	8.51	16.21	110	26.89
		IOZ23430	16.66	8.44	16.01	102	26.55
Paradoxornis conspicillatus	*conspicillatus*	IOZ30070	8.33	4.85	7.35	63	20.00
		IOZ30068	8.61	4.98	7.22	67	20.87
Paradoxornis zappeyi	*zappeyi*	IOZ58316	7.78	4.18	5.85	70	/
		IOZ60223	8.00	4.20	5.86	77	20.48
		IOZ60208	7.85	4.16	5.81	76	/
		IOZ60207	7.86	4.18	5.80	75	20.50
Paradoxornis fulvifrons	*albifacies*	IOZ35776	7.51	4.92	5.81	67	21.42
		IOZ35777	7.46	4.97	5.70	64	21.26

		IOZ35778	7.46	4.98	5.77	71	20.78
		IOZ35779	7.76	4.94	5.89	65	21.53
	cyanophrys	IOZ49819	7.58	5.01	5.82	70	21.47
Paradoxornis verreauxi	*craddocki*	IOZ49868	7.11	5.42	6.88	55	16.89
		IOZ49867	7.37	5.30	6.91	52	17.04
	verreauxi	IOZ49818	7.20	5.30	6.90	53	/
		IOZ44023	7.27	5.48	6.94	49	17.00
		IOZ17055	7.10	5.33	6.80	49	17.37
		IOZ17054	7.20	5.41	6.83	50	16.59
	craddocki	IOZ49869	7.28	5.41	6.87	53	16.77
		KIZ019945	7.30	5.40	6.80	52	18.00
		KIZ019946	7.10	5.50	6.80	53	18.00
Paradoxornis atrosuperciliaris	*atrosuperciliaris*	IOZ58140	10.31	7.58	10.45	76	24.07
		IOZ58139	10.95	7.59	10.49	86	23.54
Paradoxornis ruficeps	*ruficeps*	IOZ58141	15.63	8.16	11.12	92	28.90
		IOZ58142	14.78	8.35	12.16	91	30.22
Paradoxornis gularis	*rasus*	IOZ58143	13.94	6.51	10.60	82	24.20
		IOZ58144	14.33	6.65	10.76	79	25.99
		IOZ58145	14.21	6.57	10.58	87	25.50
	fokiensis	IOZ17080	15.08	6.81	10.63	84	25.61
		IOZ19514	15.13	6.75	10.75	83	25.94
		IOZ23467	14.77	6.70	10.62	86	/
		IOZ52050	14.86	6.77	10.79	84	25.80
	hainanus	IOZ26152	13.95	6.57	10.20	79	25.10
		IOZ26153	13.72	6.68	10.06	/	/
		IOZ6551	14.25	6.70	9.90	/	/
		IOZ43157	13.75	6.60	10.07	72	23.81
Paradoxornis heudei	*heudei*	IOZ23414	16.79	7.34	13.40	113	27.45
		IOZ23412	16.41	7.41	13.29	105	26.21
		IOZ16176	16.71	7.35	13.20	103	25.47
		IOZ23427	16.60	7.38	13.22	104	/
Paradoxornis brunneus	*brunneus*	IOZ46487	8.61	4.78	7.28	58	/
		IOZ46488	8.69	4.79	7.15	/	21.90
		IOZ48210	8.46	4.67	7.17	65	/
		IOZ48211	8.78	4.75	7.24	/	21.96
		IOZ57429	8.46	4.62	7.06	/	/

	ricketti	IOZ35789	8.42	4.65	7.25	65	/
		IOZ35790	8.41	4.65	7.21	/	/
		IOZ49815	8.21	4.56	7.08	/	18.05
		IOZ37955	8.75	4.66	7.10	121	18.41
Paradoxornis webbianus	*webbianus*	IOZ23444	8.92	4.76	6.19	49	/
		IOZ23448	8.98	4.79	6.32	62	18.70
		IOZ50430	8.79	4.70	6.15	55	18.89
		IOZ50431	8.90	4.75	6.25	65	18.91
	suffusus	IOZ19483	8.95	4.72	6.25	56	18.94
		IOZ19497	8.91	4.74	6.23	51	18.92
		IOZ20789	8.97	4.73	6.28	59	18.92
		IOZ20795	9.00	4.77	6.24	66	/
	yunnanensis	IOZ32707	8.85	4.75	6.50	58	20.32
		IOZ32708	8.91	4.77	6.48	53	18.87
	stresemanni	IOZ44013	8.88	4.74	6.96	63	18.50
		IOZ44014	8.73	4.75	6.71	64	18.55
		IOZ52241	8.89	4.81	6.83	55	18.59
	fulvicauda	IOZ6258	8.72	4.70	6.75	76	19.62
		IOZ6273	8.94	4.83	6.80	66	20.54
		IOZ6270	8.92	4.80	6.72	75	19.63
		IOZ6297	8.99	4.83	6.83	76	/
Paradoxornis alphonsianus	*alphonsianus*	IOZ47201	8.80	4.67	6.39	60	18.85
		IOZ35787	8.89	4.69	6.45	59	/
		IOZ17067	8.94	4.69	6.49	58	19.24
		/	8.92	4.69	6.38	61	18.87
Paradoxornis nipalensis	*poliotis*	KIZ012944	8.10	5.20	6.60	51	18.00
		KIZ012945	8.40	5.20	6.90	54	18.00
		KIZ011267	8.60	5.30	7.30	55	19.00
		KIZ012943	7.00	5.10	6.30	53	18.00
	beaulieui	KIZ008777	8.60	5.30	7.10	46	/
		KIZ008775	7.90	5.10	6.80	47	/
		KIZ020055	7.80	5.10	7.10	/	/
		KIZ008776	8.30	5.20	7.20	/	18.00
Paradoxornis davidianus	*davidianus*	FNU2295908	10.40	5.30	8.60	36	17.10
		FNU2295902	11.30	5.50	8.60	35	17.90
		FNU2295903	10.90	5.50	8.50	35	17.60
		FNU2295901	11.20	5.70	8.60	37	17.80

FNU2295905	11.30	5.50	8.70	39	17.60
/	11.00	5.40	8.50	39	17.70

Table S3 Different diversification models fitted to the time-calibrated species tree with parameter and support values.

	λ (speciation)	*μ* (extinction)	*additional parameters of diversity- and time-dependent models*	*t (time-shift)*	*λ2*	t2	*λ3*	t3	*λ4*	AIC	*ΔAIC*	AICc	*ΔAICc*
1) a pure birth (Yule)	0.149									27.984	2.759	28.234	1.404
2) a rate-constant-birth-death (bd) model	0.149	0								29.984	4.759	30.784	3.954
3) yule2rate	0.145			0.644	0.184					25.225	0.000	26.939	0.109
4) yule3rate	0.242			4.997	0.854	4.798	0.073			27.255	2.030	32.255	5.425
5) yule4rate	0.242			4.997	0.854	4.798	0.052	0.644	0.184	29.604	4.379	40.804	13.974
6) DDX	0.949		x= 0.826							26.030	0.805	26.830	0.000
7) DDL	0.336		K=20.940							26.305	1.081	27.105	0.275
8) SPVAR	0.572	0.095	k=0.151							29.553	4.329	31.267	4.437
9) EXVAR	0.149	0.001	z=0.001							31.984	6.760	33.698	6.868
10) BOTHVAR	0.472	0.372	k=0.132, z=0.026							31.459	6.234	33.173	6.343

DDX, DDL: initial speciation rate

SPVAR, EXVAR, BOTHVAR: initial speciation rate, final extinction rate

x= Parameter controlling the magnitude of the rate change.

K=Parameter analogous to the 'carrying capacity'

parameter of population ecology

k=Parameter of the exponential change in speciation rate

z=Parameter of the exponential change in extinction rate

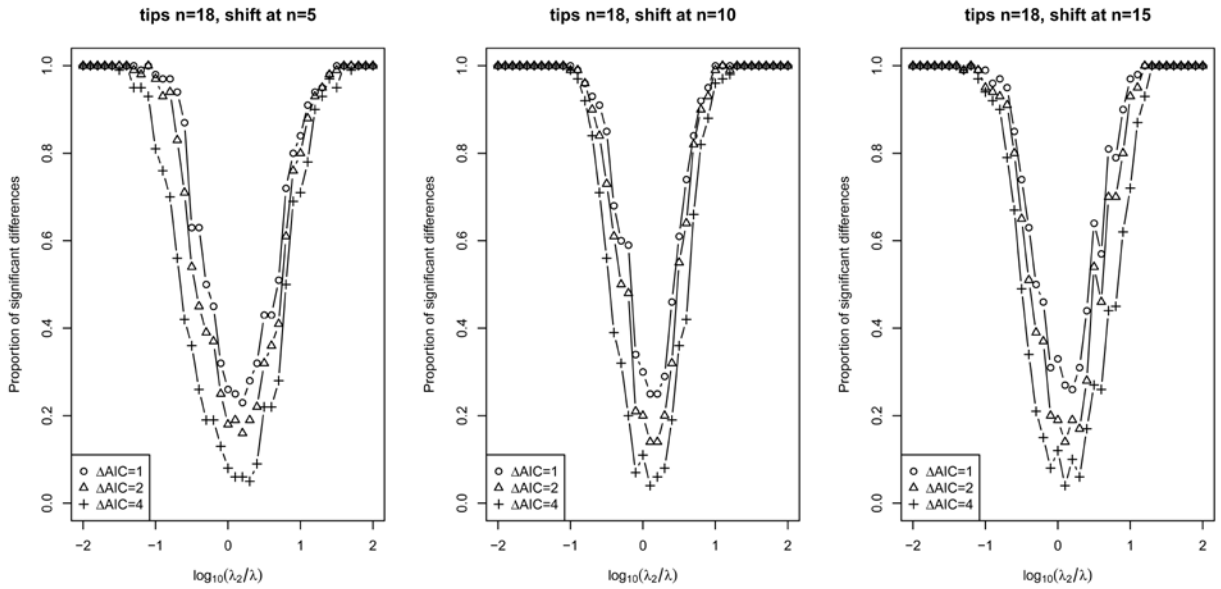

Figure S1 Proportion of cases out of 100 replicates in which a single-rate speciation model was rejected in favor of a two-rate model for trees with 18 tips. In each plot, the x-axis shows the log of the ratio between the younger rate (lambda 2) and the older rate (lambda). A ratio of zero indicates no change in rate. Results are shown for different times at which the rate shift occurred (after the appearance of 5, 10 or 15 lineages) and for different minimal AIC differences required to reject a single rate model (delta AICs of 1, 2 and 4). All simulations were performed by drawing waiting times between speciation events from an exponential distribution with rate r=l*lambda, where l is the currently extant lineages. These results suggest considerable power to detect rate shifts when changes in rate are 10-fold or more, even for "small" trees of about 18 tips.

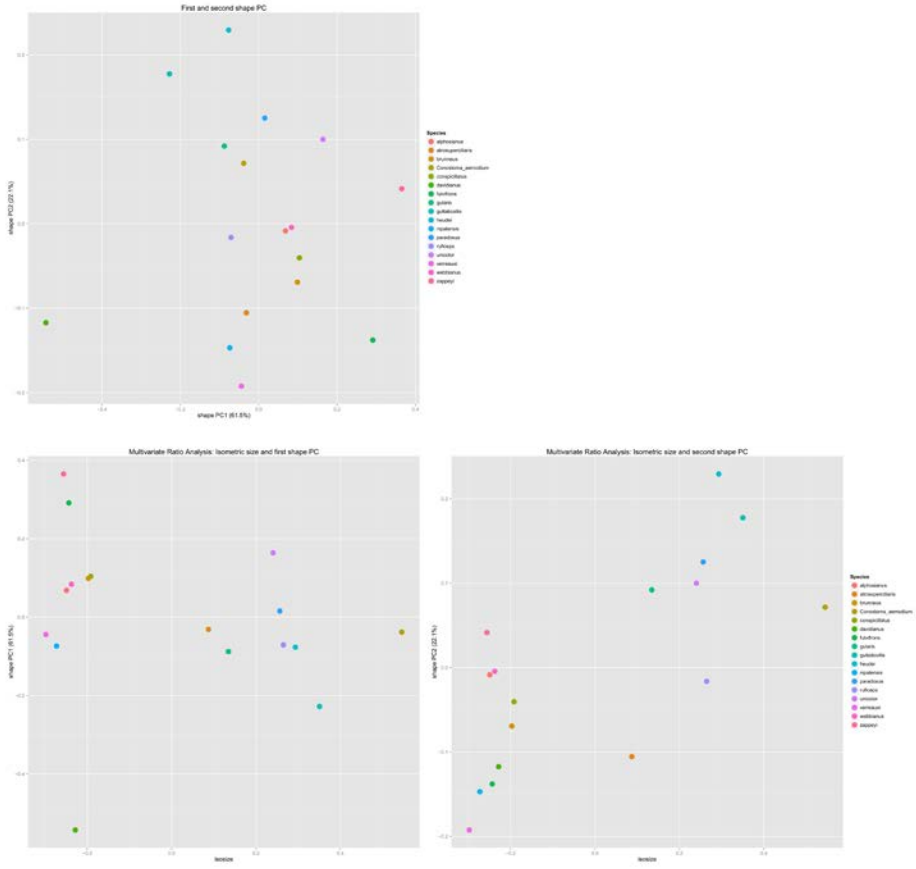

Figure S2. Scatterplot of shape PC1 against shape PC2 (top left), isosize against shape PC1 (bottom left) as well as isosize against shape PC2 bottom right.

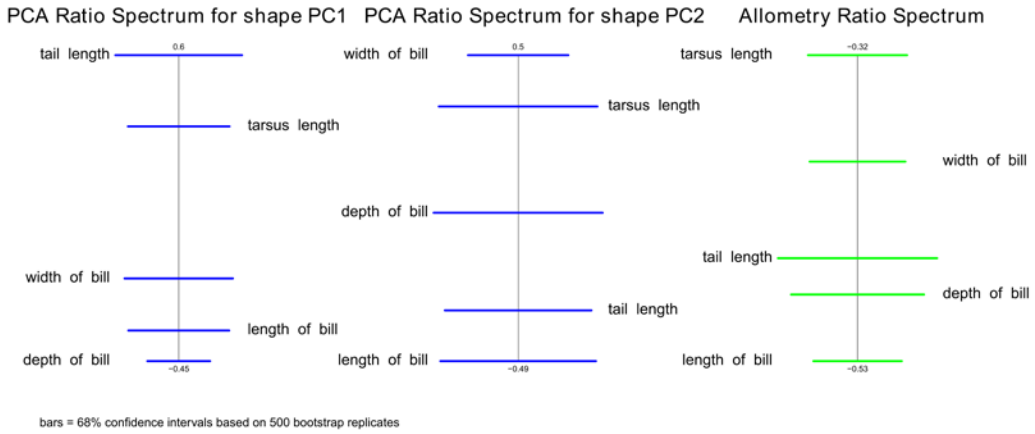

Figure S3. PCA ratio spectrum for first and second principal component in shape and allometry ratio spectrum. Ratios calculated from characters lying far apart in the ratio spectrum explain a large part of the variance of a component, while ratios of characters lying close to each other in the spectrum contribute little to the total variance (cf. Baur & Leuenberger, 2011). The allometry ratio spectrum is interpreted in accordance with the PCA ratio spectrum. The ratios calculated from characters lying furthest apart thus exhibit the most distinctive allometric behavior. While shape PC1 is dominated by the ratio of tail length and depth of bill length, shape PC2 is dominated by the ratio of width of bill and length of bill. The ratio that dominates shape PC1 and shape PC2 are only marginally affected by allometric relationships.

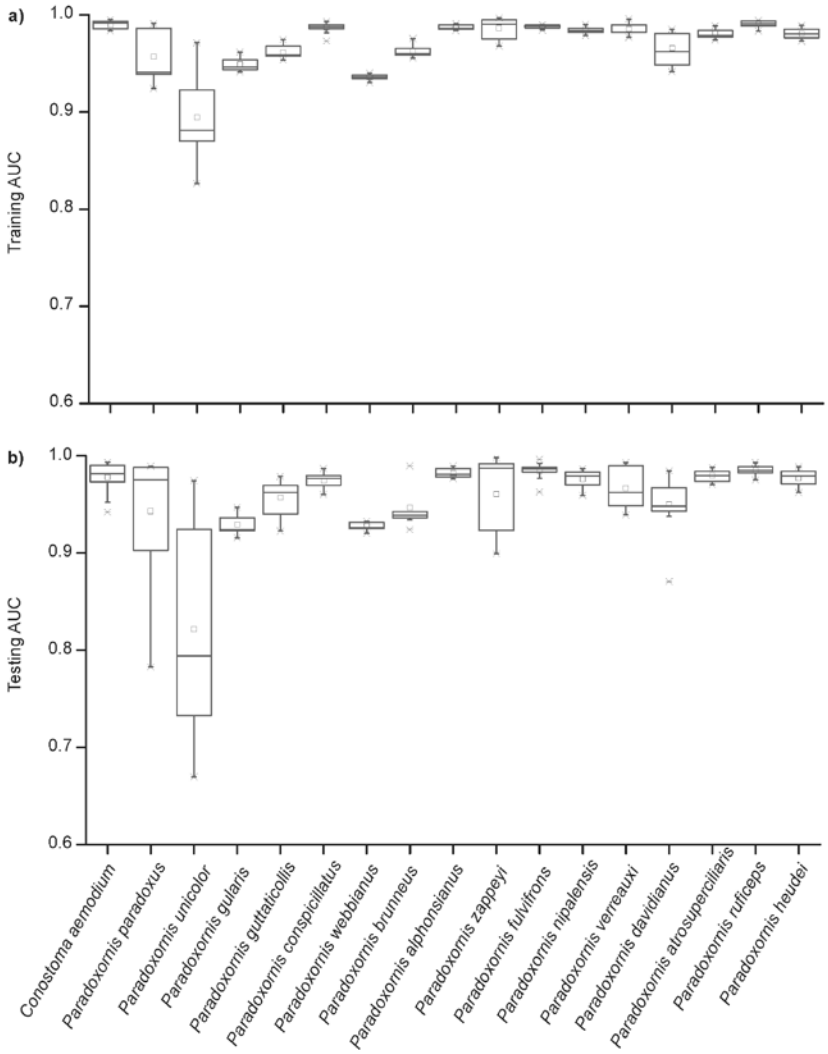

Figure S4. Discrimination ability of the Maxent model through the receiver operating characteristic curve (AUC) for parrotbill species: a) training AUC; b) testing AUC.

Figure S5. Predicted climatic suitability for parrotbill species. Values range from 1 (highest suitability) to 0 (lowest suitability). The map of distribution range in each panel (blue) represents the range limit for each species from BirdLife International and NatureServe (2014)